

A structure for quasars under the scope of polarisation

I. The UV/optical polarisation dichotomy of type-1 and type-2 AGN

F. Marin^{*} and R. W. Goosmann

Observatoire Astronomique de Strasbourg, Université de Strasbourg, CNRS, UMR 7550, 11 rue de l'Université, 67000 Strasbourg, France

Accepted 2013 September 14. Received 2013 September 13; in original form 2013 June 30

ABSTRACT

We present UV/optical spectropolarimetric modelling of the phenomenologically-based structure for quasars proposed by Elvis (2000). In this first paper of a series, we explore the continuum polarisation emerging from radiatively accelerated and bent winds that were vertically launched from the accretion disc in an active galactic nucleus (AGN). We simulate the radiative transfer occurring in Thomson scattering and dust extinction media over a range of morphological parameters and optical depths of the wind. We demonstrate that the wind geometry proposed by Elvis with a phenomenologically-derived bending angle of $\theta = 60^\circ$ still underestimates the observed optical polarisation percentage of type-1 and type-2 AGN and does not yet reproduce the expected dichotomy of the polarisation position angle. To recover the observed polarisation properties, a smaller bending angle and some amount of dust shielding in the equatorial region should be considered. A two-phase outflow is found to generate both the observed polarisation dichotomy and acceptable levels of polarisation degree if the wind has a bending angle $\theta = 45^\circ$, and the conical shells have a half-opening angle of $3^\circ < \delta\theta < 10^\circ$. The absorbing dust column at the wind base should be in the range of $1 < \tau_{dust} \leq 4$ (τ being integrated over 2000 – 8000 Å). Straightforward observational tests from spectropolarimetry and from determining the number density of different AGN types can be performed to further constrain the wind geometry.

Key words: Polarisation – scattering – radiative transfer – galaxies: active – galaxies: Seyfert

1 INTRODUCTION

While the topic of quasar research started in the beginning of the twentieth century (Fath 1909), it took nearly ninety years to build up a coherent, unifying model for radio-quiet AGN¹ (Antonucci 1993). It is now widely accepted that a supermassive black hole (SMBH) with mass ranging from 10^6 to $10^{10} M_\odot$ is surrounded by an accretion disc and its associated corona, who radiate a continuum spectra from the soft X-ray energy to the near-infrared waveband. Broad line signatures are thought to arise from high velocity gas trapped close to the equatorial plane between the accretion disc and a surrounding, optically thick, circumnuclear dust medium. This "dusty torus" is thought to collimate ejection

winds along the polar direction, where narrow line features are expected to be produced by distant, low velocity outflows.

According to the unified scheme, many of the AGN observational characteristics can be explained by an inclination effect rather than intrinsic composition differences. However, the exact morphology of the inner AGN regions remains highly debated due to a wide panel of observational emission and absorption line features. If cylinder-like, spinning, equatorial reprocessing regions where initially used to model the broadening of the emission lines in Seyfert-1 objects (see Osterbrock 1991 for a review), it is now admitted that the morphology of the broad line region is by far more complex (e.g. Davidson & Netzer 1979; Mathews & Capriotti 1985; Shields 1977; Eracleous 2006; Gaskell 2009). In this picture, the central, ionising source is surrounded by a roughly spherical distribution of clumps in Keplerian motion, situated at the outermost areas of the accretion disc (Gaskell & Goosmann 2013). Similar assumptions about the clumpy nature of the narrow line regions (Capetti et al. 1995; Ogle et al.

^{*} E-mail: frederic.marin@astro.unistra.fr

¹ In this paper we only consider radio-quiet AGN models, as the presence of a relativistic jet would lead to a more complicated spectropolarimetric picture by adding intrinsically highly polarised synchrotron emission

2003) increase the difficulty of the challenging but necessary goal of drawing a unifying model for the sub-parsec regions of quasars.

In this context, Elvis (2000) developed a phenomenologically-based model to explain the wide variety of emission and absorption features in AGN spectra, assuming a simple outflowing structure. The model presented by Elvis (2000) assumes a flow of warm, highly ionised matter (WHIM) that is launched from an accretion disc over a small range of radii and then bent outward and driven into a radial direction by radiation pressure (see Fig. 1 and Elvis 2000). Certain aspects of this phenomenologically-derived structure can be directly tested from number counts of type-1 and type-2 AGN or the relative number of broad absorption line (BAL) versus narrow absorption line (NAL) objects. The wind structure surrounds the irradiating accretion disc and gives rise to a reprocessing spectrum that varies with the disc luminosity and the viewing angle of the observer. Time-resolved spectroscopy therefore is a powerful tool to test the model against the observations, but this technique may not be sufficiently sensitive to the outflow geometry and dynamics.

To extend the comparison of the outflow model to the observations somewhat further, spectropolarimetric data of AGN can be explored. In the optical/UV band, the polarisation of radio-quiet AGN is mostly determined by reprocessing and strongly depends on the scattering geometry. We expect BAL objects to be generally more highly polarized than non-BAL QSOs (Ogle et al. 1999) and NAL Seyfert-like galaxies to show polarisation parallel to the axis of the torus associated with polarisation degrees inferior to unity (Smith et al. 2002). Spectropolarimetric observations of nearby Seyfert galaxies showed that there is an observational dichotomy between type-1 and type-2 AGN: a large fraction of AGN seen by the pole (type-1) show a polarisation position angle oriented parallel to the system axis, while edge-on objects (type-2) exhibit a perpendicular polarisation position angle (Antonucci 1983). When a polarisation model is provided, one of its goals is to reproduce the observed dichotomy, where parallel polarisation is thought to originate close to the SMBH, while perpendicular polarisation emerges from the circumnuclear matter or the ionised winds (see references and modelling in Goosmann & Gaskell 2007; Marin et al. 2012). Direct *Hubble Space Telescope* (HST) polarization imaging of NGC 1068 and Markarian 477 showed that perpendicular polarisation can also emerge from scattering clumps situated 10 to 100 pc away from the innermost regions (Capetti et al. 1995; Kishimoto 1999; Kishimoto et al. 2002); in these cases, the necessity to reproduce type-2 perpendicular polarisation is less critical. However, the production of parallel polarisation in type-1 AGN is a rather important challenge, as it might give us an insight of the intrinsic spectral shape of the central engine. The detection of a Balmer absorption edge in a few quasars (Kishimoto et al. 2003, 2004), thought to originates interior to the BLR, strengthens the role of parallel polarisation as a tool to constrain the geometry and the composition of reprocessing and scattering media close to the SMBH (Kishimoto et al. 2008). This continues to be very relevant in AGN research where geometry is a key parameter for unification theories (Antonucci & Miller 1985; Antonucci 1993; Elvis 2000).

In the present work, we model the polarisation properties produced by radiative reprocessing inside the structure of quasars as suggested by Elvis (2000). We focus on the continuum polarisation at optical and ultraviolet wavelengths and we test if the outflow model can reproduce the observed dichotomy with respect to the polarisation position angle (Antonucci 1983, 1984; Smith et al. 2002). The remainder of the paper is organised as follows: in Sect. 2 we present and analyse spectropolarimetric simulations of disc-born outflows for different model parameters. In Sect. 3 we discuss our results and relate them to the observational constraints before drawing our conclusions in Sect. 4.

2 EXPLORING THE STRUCTURE FOR QUASARS BY SPECTROPOLARIMETRY

2.1 Radiative transfer code and model geometry

To study the model of Elvis (2000), we apply the version 1.2 of Monte Carlo radiative transfer code STOKES presented in Goosmann & Gaskell (2007) and upgraded by Marin et al. (2012). This modelling suite coherently treats three-dimensional transfer and multiple reprocessing between emitting and scattering regions and includes a treatment of polarisation. The model space is surrounded by a spherical web of virtual detectors. The detectors record the wavelength, intensity and polarisation state of each photon. The latest-to-date version of STOKES also generates polarisation images with the photons being projected onto the observer's plane of the sky and then stored in planar coordinates. The net intensity, polarisation degree P and polarisation position angle ψ as a function of wavelength are then computed by summing up the Stokes vectors of all detected photons in a given spectral and spatial bin. The spectra can be evaluated at each viewing direction in the polar and azimuthal direction i and ϕ . Note that a position angle $\psi = 0^\circ$ denotes a polarisation state with the \vec{E} -vector oscillating in a perpendicular direction with respect to the symmetry axis of the wind, while for $\psi = 90^\circ$ the \vec{E} -vector is parallel to the (projected) wind axis.

We simulate the radiative transfer through the structure for quasars as proposed by Elvis (2000) by constructing continuous outflow regions that can be filled with electrons or dust or a combination of the two at uniform density. Assuming a uniform density certainly is an oversimplification and we are going to release this condition in future work. For now, we only perform the most basic polarisation test of the wind model. For all models presented in this paper, the equatorial emitting region will be defined as an isotropic, disc-like source emitting an unpolarised spectrum with a power-law spectral energy distribution $F_\star \propto \nu^{-\alpha}$ and $\alpha = 1$. The model geometry is summarised in Fig. 1: the wind arises from the accretion disc at a distance r_1 of 0.0032 pc (10^{16} cm) and is bent into a direction of $\theta = 60^\circ$ relative to the model symmetry axis. The range of radii where the flow arises from the accretion disc is parametrised by $r_2 = 0.00032$ pc (10^{15} cm). Finally, the half-opening angle $\delta\theta$ of the wind is 3° and the flow extends up to $r_3 = 0.032$ pc (10^{17} cm). It is instructive to express these distances in units of the gravitational radius (R_G) for a fiducial black hole mass of $\sim 10^7 M_\odot$ (such as in NGC 5548), as well

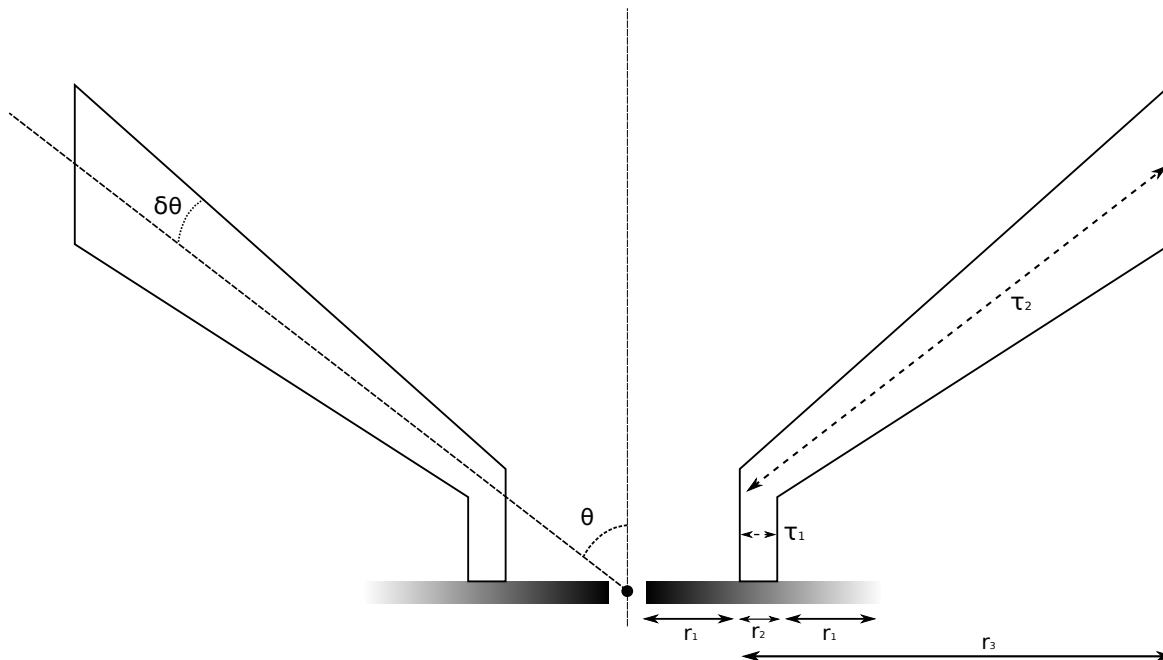


Figure 1. Schematic view of the structure proposed by Elvis (2000) and implemented in the STOKES model. The outflow arises vertically from the accreting disc and is bent outward by radiation pressure along a 60° direction relative to the model symmetry axis. The half-opening angle of the wind extension is 3° . The radial optical depths of the wind base and of the outflowing material are set to by τ_1 and τ_2 respectively.

Radius	pc	cm	R_G	$T_{\tau,K}$	R_{BLR}
r_1	0.0032	10^{16}	6684	0.08	0.91
r_2	0.00032	10^{15}	668	0.008	0.091
r_3	0.032	10^{17}	66840	0.8	9.1

Table 1. Parameters of the model expressed in units of gravitational radius R_G (for a black hole mass of $\sim 10^7 M_\odot$), dust sublimation radius $T_{\tau,K}$ and BLR radius R_{BLR} . See text for further details.

as in units of the dust sublimation radius ($T_{\tau,K}$, $T = 1500$ K, Suganuma et al. 2006; Kishimoto et al. 2007) and BLR radius (R_{BLR} , Bentz et al. 2009). We estimated $T_{\tau,K}$ and R_{BLR} from NGC 5548’s near-IR reverberation measurements and reverberation mapping of $H\beta$, respectively. Converted radii, given in Tab. 1, imply that the phenomenological outflow derived by Elvis (2000) arises below the dust formation radius and the BLR is likely to form closely beyond the inner part of the wind. The extension of the wind covers a large fraction of the BLR, essentially obscuring the highly ionized clouds close to the central engine.

2.2 The warm, highly ionised medium

2.2.1 Testing the electron-dominated outflows

We assume that the WHIM is mainly composed of ionised gas with a Thomson optical depth τ of the order of unity along the conical outflowing direction. This wind extends out to several parsec and can be associated with the “ionisation cones” observed in nearby Seyfert-2 galaxies (Capetti

et al. 1995; Axon et al. 1996; Osterbrock 1991). To investigate the scattering properties and the resulting spectra and polarisation from the WHIM, we first consider a uniform-density, continuous medium made of electrons. The Thomson optical depth at the wind base and inside the conical, outflowing direction are set to $\tau_1 \sim 0.02$ ($n_e = 3 \times 10^7$) and $\tau_2 \sim 2$ ($n_e = 2.6 \times 10^6$), respectively. Such an optical depth is in agreement with observational measurements (Packham et al. 1997; Ogle et al. 2003) and also suggested by polarisation modelling work on NGC 1068 (Miller et al. 1991; Young et al. 1995; Goosmann & Matt 2011).

In Fig. 2, we plot the simulated spectropolarimetric results across the $2000 - 8000 \text{ \AA}$ wave band and as a function of the observer’s viewing angle. We consider three different lines-of-sight : one along a polar inclination (9°), one passing through the outflowing wind (61°), and one along an extreme equatorial inclination (89°). The inclination of the system is defined with respect to the symmetry axis of the model. The polar and equatorial lines of sight do not cross the extended wind and the fraction F/F_* of the central flux, F_* , remains similar for both inclinations. At intermediate inclinations, however, a significant fraction of the radiation is scattered out of the line-of-sight by the optically thick wind. The polarisation percentage at all three viewing directions is wavelength-independent, as it is expected for Thomson scattering, and the polarisation position angle is $\psi = 90^\circ$ (parallel polarisation) for all cases. The polarisation percentage P is very low at polar viewing angles and then rises with i . It increases to 0.05 % when looking through the ex-

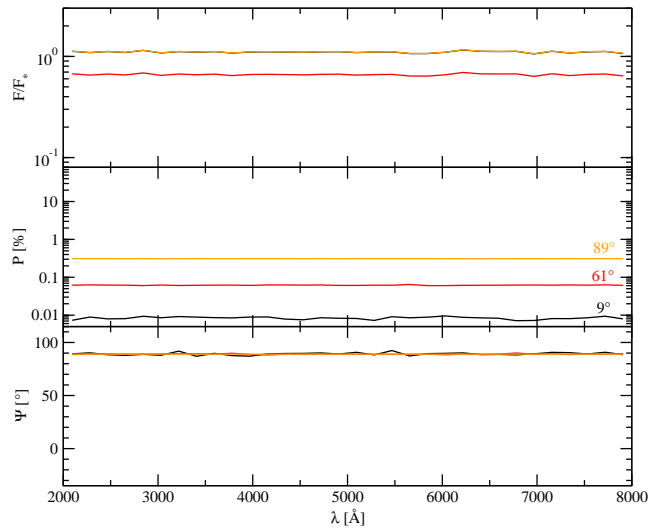


Figure 2. Modelling an electron-filled structure for quasars outflow using a uniform model such as in Fig. 1, seen at different viewing inclinations, i (black : 9° – red : 61° – orange : 89°). *Top*: the fraction, F/F_* of the central flux; *middle*: polarisation, P ; *bottom*: polarisation angle, ψ .

tended wind and then further to about 0.3 % for an edge-on line-of-sight.

The corresponding polarisation images are shown in Fig. 3. The 60×60 spatial bins compile the polarisation properties integrated across the whole wave band of 2000 – 8000 Å. Each pixel is labelled by its projected coordinates x and y (in parsecs) with respect to the centre of the model space. The polarised flux PF/F_* is colour-coded and the orientation and length of a vector drawn in black at the centre of each pixel represent the ψ and P values, respectively. The degree of polarisation is maximal for a full-length vector (size of a spatial bin); the length variation is proportional to P .

Inspection of the polarisation images is helpful to understand the net polarisation properties as a function of the viewing angle: at a polar viewing direction (Fig. 3, top), the central source irradiates the outflow funnel, which causes a weak polarised flux in the vicinity of the model centre. However, the spatial distribution of polarisation position angles remains close to being symmetric with respect to the centre and therefore the resulting net polarisation at a low viewing angle is weak. Furthermore, the polarisation is strongly diminished by the diluting flux coming from the continuum source that is directly visible at low inclinations. The resulting polarisation position angle at $\psi = 90^\circ$ is determined by the geometry as the wind is rather flat ($\theta = 60^\circ$) and therefore favours scattering close to the equatorial plane. Equatorial scattering produces parallel polarisation and was suggested early-on to play an important role in producing the polarisation properties of type-1 AGN (Antonucci 1984).

At $i = 61^\circ$ (Fig. 3, middle) the line-of-sight passes through the extended winds. The net polarised flux now comprises a strong component seen in transmission. While the wind base is optically thin, the scattering optical depth along the line-of-sight is significant and the latter thus contributes strongly to the net polarisation. The interface between the inner funnel of the torus and the extended winds

is traced by a sharp gradient in polarised flux. The inner (outer) surfaces of the upper (lower) part of the outflow are visible in reflection, but due to their low optical depth in the poloidal direction the scattering is inefficient and does not produce much polarised flux.

Finally, the equatorial view of the model at $i = 89^\circ$ (Fig. 3, bottom) allows us to recover the edge-on morphology of the system. The polarised flux emerging from the wind base and its extensions is significantly higher than at the intermediate view. The boundaries of the extended winds trace out an X-shaped structure that extends far out and produces strong polarisation. These regions have a higher polarisation efficiency because they present a significant optical depth along the line of sight and favour a scattering angle around 90° with respect to the continuum source.

The polarisation position angle ψ is equal to 90° for all viewing angles, indicating that the polarisation angle is oriented parallel to the symmetry axis of the system.

We remark that adopting the exact geometry suggested in Elvis (2000) for a pure electron-scattering medium underestimates the observed optical polarisation percentage of type-1 and type-2 AGN. The wavelength-independent continuum polarisation induced by the WHIM produces a polarisation position angle $\psi = 90^\circ$ at all viewing angles, whereas in type-2 AGN the resulting polarisation should be perpendicular. It is then necessary to look at more realisations of the model for slightly different parametrisations.

2.2.2 Exploring different bending and opening angles of the wind

We continue our investigation by exploring different angles θ and $\delta\theta$ of the wind. To obtain a more narrow cone with respect to the default parametrisation used in Sect. 2.2.1, it is necessary to lower the bending angle θ while the wind extensions become thicker when increasing the half-opening angle $\delta\theta$. We systematically explore the response in polarisation for a range of both angles and summarise the results in Fig. 4. Since the polarisation of electron scattering is wavelength-independent we now plot the wavelength-integrated polarisation degree as a function of the viewing angle. Note that we apply a sign convention for P that expresses the orientation of the polarisation position angle: for positive P , the \vec{E} -vector is perpendicular to the wind axis, while for negative P the polarisation is parallel (intermediate orientations of the net polarisation are impossible due to symmetry reasons).

For $\theta = 75^\circ$ the model produces polarisation degrees that are low at small viewing angles and moderate, up to 15 %, for higher inclinations. The normalisation of P rises with $\delta\theta$. There is no dichotomy for the polarisation angle as the \vec{E} -vector is always parallel to the projected axis. The case of $\theta = 60^\circ$ with $\delta\theta = 3^\circ$ is discussed in the previous section. It turns out that increasing $\delta\theta$ can change the dichotomy of the polarisation position angle and even produce three or four different regimes at low, intermediate and large viewing angles. The polarisation then turns out to be parallel for a face-on and edge-on view and perpendicular along a line-of-sight through the wind. Further narrowing the bending angle to $\theta = 45^\circ$ increases the trend to have multiple regimes for the polarisation angle that now occur

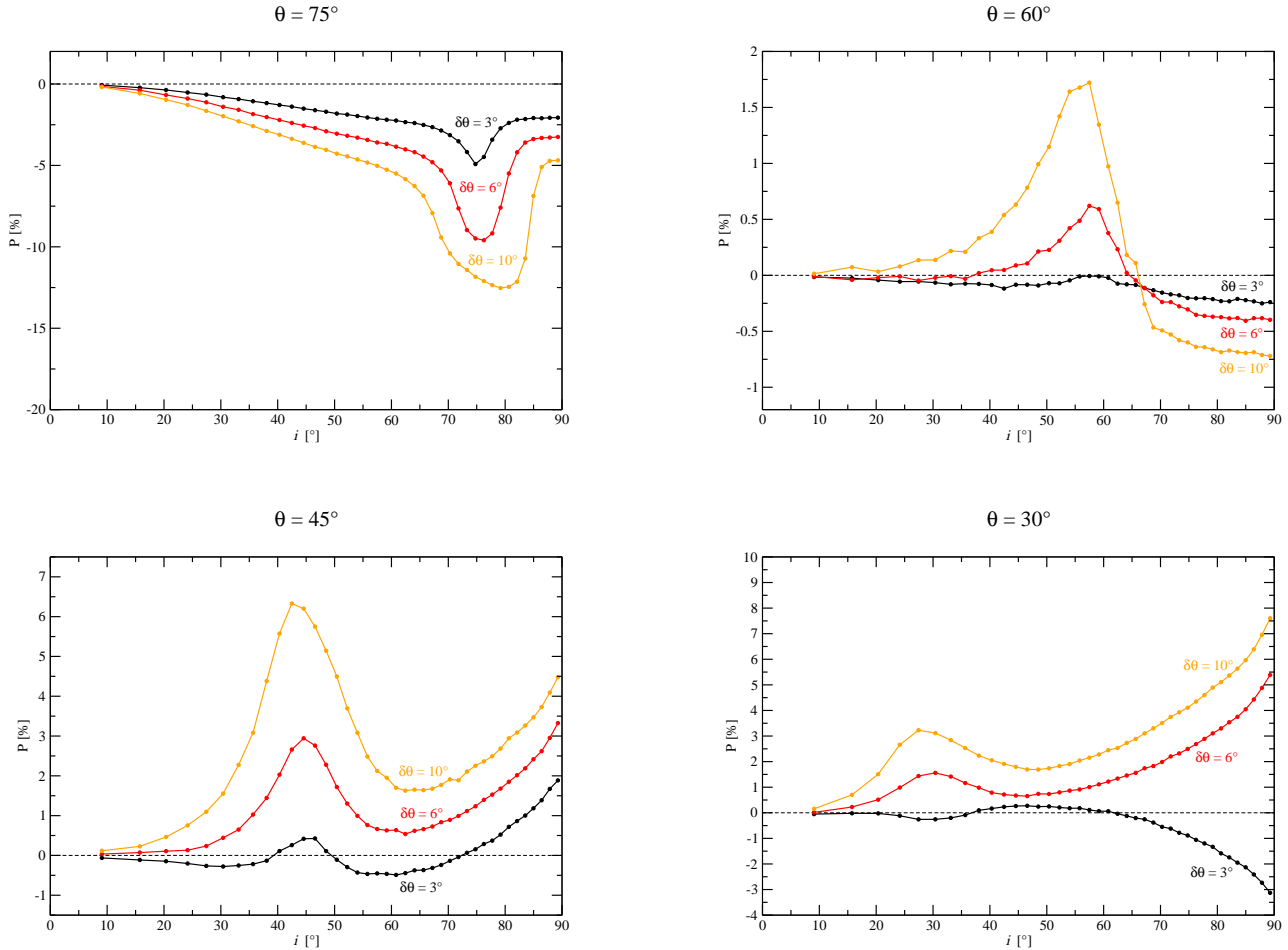


Figure 4. Investigating the polarisation response of the quasar’s structure according to the observer’s viewing angle i , at four different wind bending angles θ and three outflows opening angle $\delta\theta$ (black : $\delta\theta = 3^\circ$ – red : $\delta\theta = 6^\circ$ – orange : $\delta\theta = 10^\circ$). *Top-left:* $\theta = 75^\circ$; *top-right:* $\theta = 60^\circ$; *bottom-left:* $\theta = 45^\circ$; *bottom-right:* $\theta = 30^\circ$.

even for the smallest opening angle of $\delta\theta = 3^\circ$. It also reinforces the polarisation degree for parallel polarisation until an optimum is reached and the trend becomes inverted (see the case of $\theta = 30^\circ$).

An important motivation for the model by Elvis (2000) was given by the observed number distribution of quasars with narrow, ionised absorption lines in the UV and X-ray band versus BAL- and non-NAL objects. The BAL objects are assumed to be seen along the conical wind, the NAL objects on a line of sight that crosses the optically thin wind base. Quasars with NALs are type-1 AGN and therefore preferentially have a parallel polarisation in the optical. Interestingly, there is a parameter range for which our modelling allows for the existence of parallel polarisation at low inclinations (non-NAL, type-1 AGN with low parallel polarisation) and high-inclinations (NAL, type-1 AGN with significant parallel polarisation). In between these inclinations the line of sight points toward a BAL objects with considerable perpendicular polarisation. Immediate observational tests for the number distribution of BAL, NAL, and non-NAL quasars can be performed to test the

possible angles θ and $\delta\theta$.

An interesting challenge to the wind model by Elvis (2000) is the presence of obscured, type-2 AGN without broad absorption lines and a ubiquitous perpendicular polarisation. These objects may be accounted for by adding dust shielding at certain inclinations to the model. The dust may exist on the far-side of the wind where the temperature drops below the sublimation temperature. We are going to investigate to such scenarios in the following.

2.3 Dust in the wind

The structure for quasars analysed here may also account for the extended narrow line regions found at greater distances from the central engine. They are supposed to be the extensions of the ionised outflow, beyond the sublimation radius where dust can survive. However, the presence of dust originating close to the accretion disc remains theoretically possible according to Czerny & Hryniewicz (2012), who demonstrated that dust can be formed in accretion

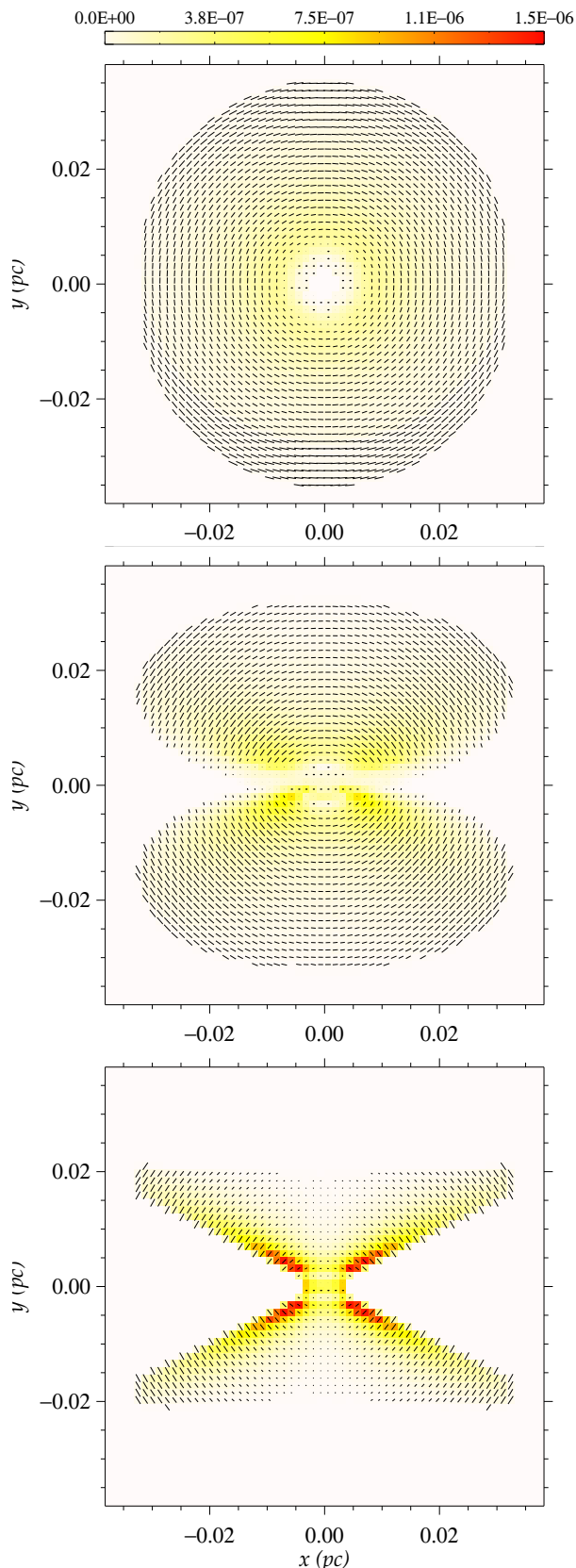


Figure 3. Modelled images of the PF/F_* for an electron-filled, scattering outflow as presented in Fig. 1. The polarised flux, PF/F_* , is colour-coded and integrated over the wavelength band. *Top:* image at $i \sim 9^\circ$; *middle:* $i \sim 61^\circ$; *bottom:* $i \sim 89^\circ$.

disc atmospheres. Dust rises similarly to the electronic disc-born wind, but is soon evaporated by the central irradiation source (Elvis 2012). Knowing that a large fraction of the thermal, infrared emission observed in low-luminosity AGN (LLAGN) is associated with the presence of dusty matter (Edelson et al. 1987), Elvis (2000) suggested that a part of the BAL flow may be obscured by a dust region that is still close to the active nucleus. It is a natural explanation of the absence of BAL in Seyfert-like galaxies and fits in with the observed presence of dusty NLR clouds at larger distances from the irradiation source.

We simulate the BAL obscuring wind using our previous WHIM model (see Sect. 2.2) and adding two cylindrically shaped extinction regions to the outer edge of the flow. The dusty wind originates at $r_3 = 0.032$ pc ($0.8 T_{7,K}$) and is of moderate optical depth ($\tau_3 \sim 1$) in order to allow the radiation to partially escape along intermediate viewing angles. The model is summarised in Fig. 5). The dust composition and grain size distribution represents an average dust type of our Milky Way (see Mathis et al. 1977; Wolf & Henning 1999; Goosmann & Gaskell 2007).

The resulting total flux spectra for polar and equatorial viewing angles (Fig. 6) are similar to those for the WHIM model (Fig. 2), indicating that Thomson scattering is the predominant reprocessing mechanism occurring at these inclinations. The impact of the dust on F/F_* remains marginal except when the observer’s line-of-sight crosses the outflowing direction ($i = 61^\circ$). The flux then becomes wavelength-dependent and increases towards the red, but with respect to the pure WHIM case it does not suffer from heavy absorption due to the moderate opacity of the dusty wind. The impact of the dust clouds is particularly visible in the percentage of polarisation. At polar inclinations, P remains below 0.05 % and is nearly wavelength-independent. At equatorial inclinations, P is at its maximum (~ 0.3 %) and again wavelength-independent. However, at an intermediate inclination, the escaping radiation crosses the dust atmosphere and presents the characteristic wavelength-dependent polarisation signal. The net polarisation degree is higher than for the pure WHIM model as photons have to scatter into the line-of-sight; P drops from 0.2 % to 0.02 % in the blue part of the spectrum and then rises back to 0.2 % in the red. This peculiar dip is connected to a switch of the polarisation position angle, from 0° to 90° , as the Mie scattering phase function becomes more forward-dominated and the overall scattering geometry thus changes towards shorter wavelengths. In this regard, the wavelength-dependent impact of dust scattering onto the polarisation position angle may serve as a tracer of the optical thickness of the obscuring region along the outflowing direction. At all other inclinations and wavelengths of the system the polarisation position angle is parallel to the system axis.

Thus, adding dust to the distant parts of the wind helps P to remain globally low, below 0.3 % (which is in agreement with the observations of non-BAL radio-quiet AGN (Berriman et al. 1990) where a mean P value of 0.5 % was found) but does not help to produce the dichotomy of the polarisation position angle in the optical.

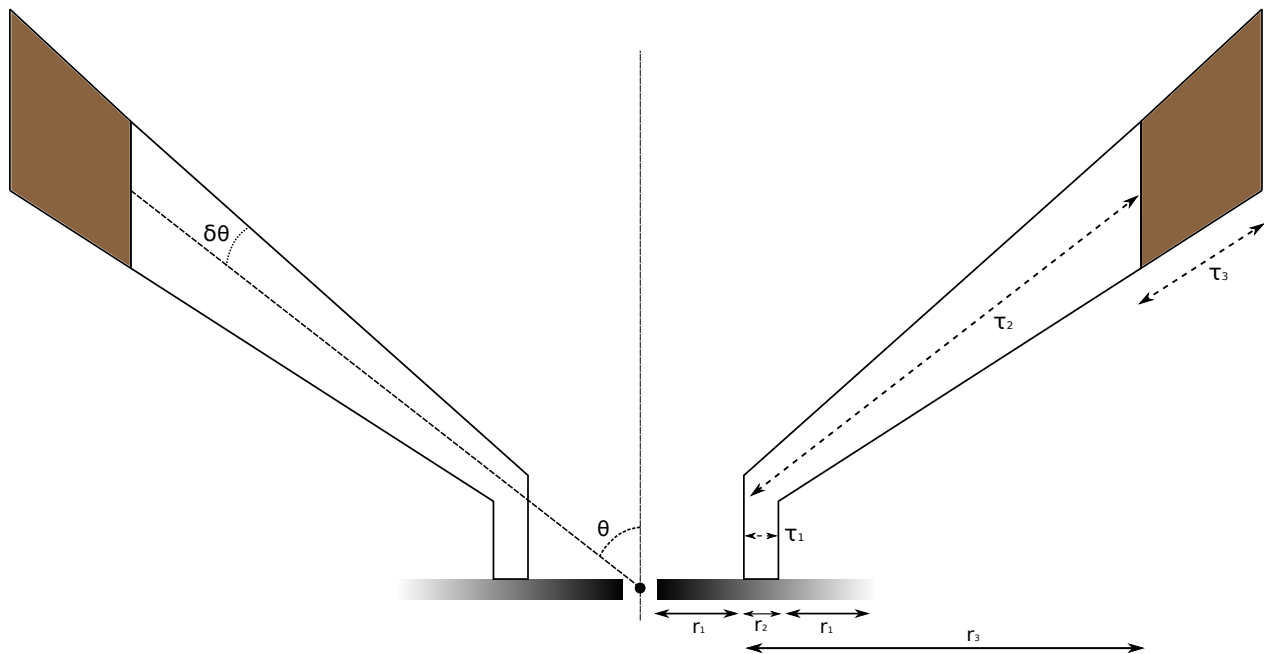


Figure 5. Investigating the presence of dust in low luminosity objects. The brownish medium represents the dusty medium, preventing the BAL from being seen in Seyfert-2 galaxies.

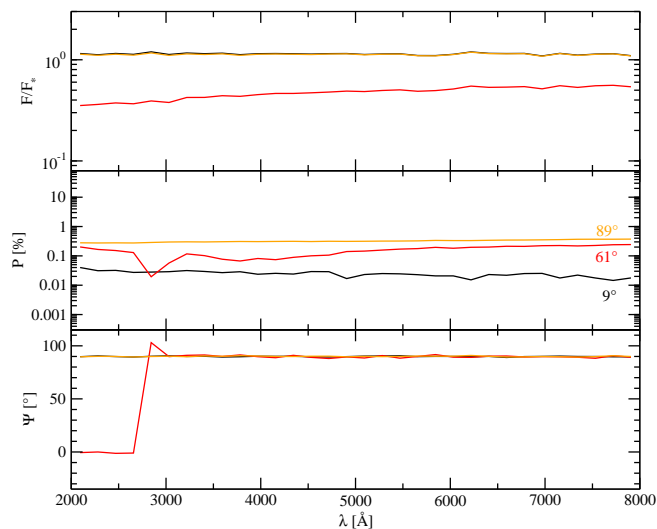


Figure 6. Modelling an obscured structure for quasars outflow where BAL are seen through a dusty medium of $\tau_{dust} \sim 1$. The model, presented in Fig. 5, is seen at different viewing inclinations, i (black : 9° – red : 61° – orange : 89°). *Top*: the fraction, F/F_* of the central flux; *middle*: polarisation, P ; *bottom*: polarisation angle, ψ .

2.4 A two-phase medium

An important test of the structure for quasars is to reproduce the polarisation position angle dichotomy observed in AGN (Antonucci 1983, 1984); our results in Sect. 2.2.2 have proven that a pure WHIM is yet inadequate to explain the switch in polarisation position angle between type-1 and type-2 AGN. In the context of Seyfert-2 AGN, the addi-

tional presence of dust close to the equatorial plane is suggested as a physical possibility (Czerny & Hryniewicz 2012). Shielded from the full continuum by the WHIM, dust can rise from the disc and survive long enough to impact the radiation across a significant solid angle around the equatorial plane. Such an absorbing medium would be less ionised than the high ionisation BEL region, giving rise to low-ionisation line emission, such as in NGC 5548 where the MgII lines are thought to arise from several light-months away from the irradiating source (Elvis 2000). However, the equatorial dust should also suppress the parallel polarisation signal at intermediate and equatorial viewing angles.

In the following, we investigate the polarisation properties of a two-phase structure, where the highly ionised inner flow self-shields radially a cold absorbing flow arising farther away from the continuum source. Such a medium should be optically thin at some viewing angle in order to allow for the detection of NAL signatures above the equatorial dust lane, but not too optically thin to prevent the production of parallel polarisation at other inclinations.

2.4.1 Modelling two-phase outflows

We adopt the morphology proposed by Elvis (2000) for NGC 5548 to explain the high/low ionisation BEL regions. Of course, dust would not survive in the BLR, so the dusty wind we define here actually needs to be farther away from the centre or remain cold by efficient shielding in the WHIM and BLR. The model geometry is presented in Fig. 7 and we fix $\tau_1 \sim 0.02$, $\tau_2 \sim 2$, $\tau_3 \sim 40$ and $\tau_4 \sim 4000$ (τ being integrated over the 2000 - 8000 Å band). The bending angle of the WHIM, $\theta = \theta_1$, is equal to 60° and $\theta_2 = \theta_1 + 2\delta\theta$. Similarly to our previous modelling, $\delta\theta = 3^\circ$. According to Elvis (2000), $r_1 = 0.0032$ pc, $r_2 = 0.00032$ pc, $r_3 = 0.032$ pc

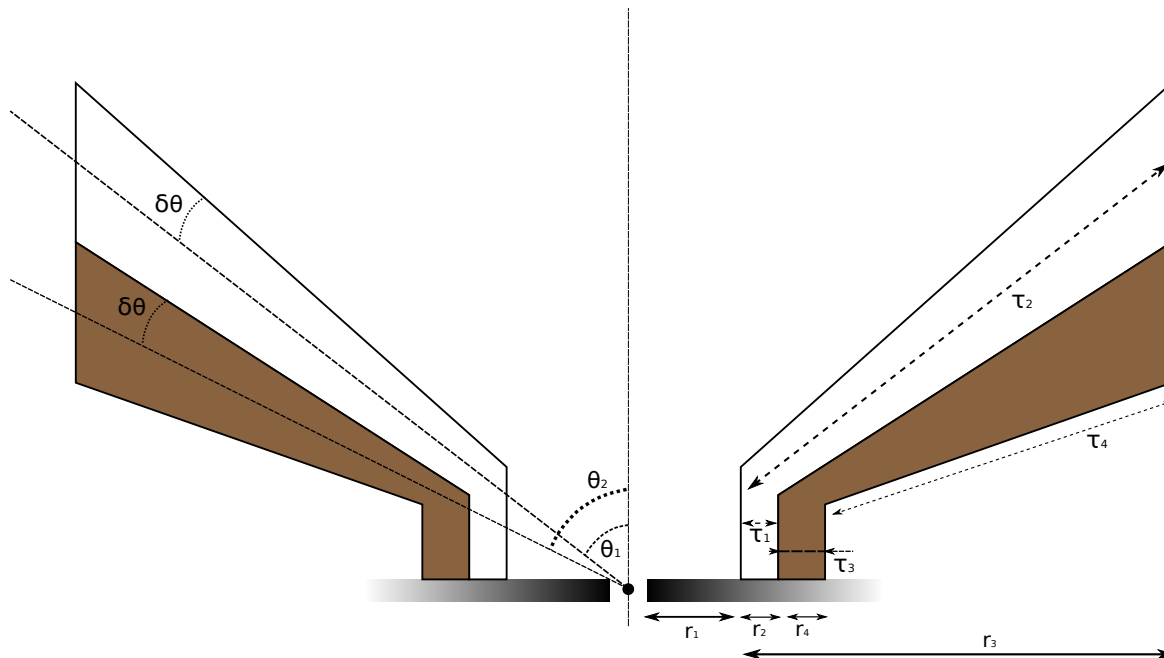


Figure 7. A two-phased medium where the cool WHIM outflow is composed of dust.

and $r_4 = 0.00608 \text{ pc} (1.88 \times 10^{16} \text{ cm} = 12700 R_G = 0.15 T_{\tau,K} = 1.74 R_{\text{BLR}})$.

To consider a more physical emission geometry, we replace the radiating disc by a point-like source. With the flux intensity decreasing like r^{-3} from the centre, most of the radiation comes from the inner part of the emitting disc. When comparing different realisations of the modelling, we find, however, that the size of the emission region does not have a major impact on the spectropolarimetric results. We now also include the fact that the inner accretion flow allows for Thomson scattering and we define a geometrically flat, flared-disc region, with optical depth $\tau \sim 1$ along the equator. This reprocessing region was proposed early on by Antonucci (1984) to explain the presence of parallel polarisation in type-1 AGN, and a complete description of its polarisation properties can be found in Goosmann & Gaskell (2007). The flared morphology is in agreement with the theory of accretion discs (Shakura & Sunyaev 1973) and will strengthen the production of parallel polarisation, with a maximum polarisation degree of up to a few percent (Marin et al. 2012). However, we checked that it only marginally contributes to the production of parallel polarisation, the bulk of it emerging from the double wind structure.

The spectropolarimetric modelling results are plotted in Fig. 8. Interestingly, the polar viewing angle shows a maximal and wavelength-independent flux in comparison with other inclinations, as expected from observations of radio-quiet, type-1 AGN. The impact of dust is visible by absorption and anisotropic scattering processes in intermediate and equatorial inclinations, where the obscured flux is a hundred times lower than at polar lines-of-sight. The percentage of polarisation is minimal for polar inclinations ($P \approx 0.01 \%$) and maximal for equatorial viewing angles

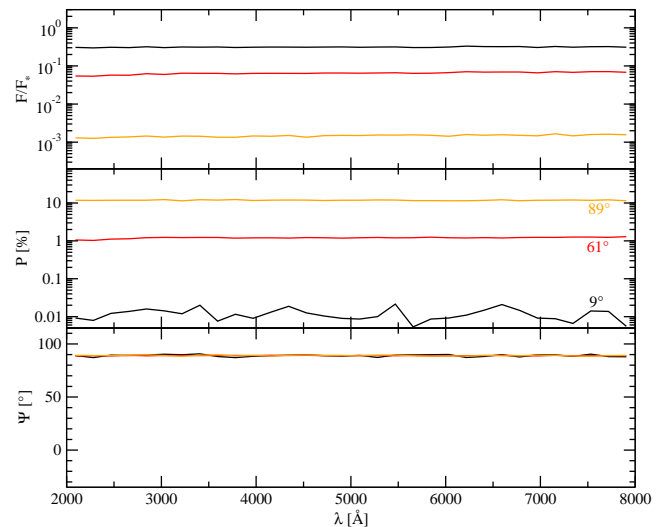


Figure 8. Modelling a two-phased quasars outflow where the cool WHIM outflow is composed of an optically thick dust medium, using a uniform model such as in Fig. 7, seen at different viewing inclinations, i (black : 9° - red : 61° - orange : 89°). *Top*: the fraction, F/F_* of the central flux; *middle*: polarisation, P ; *bottom*: polarisation angle, ψ .

($P \approx 10 \%$). Along the direction of the outflow, the polarisation ranges around 1% , is wavelength-independent, and oriented parallel to the projected axis of the model. The position angle is the same at other inclinations and the expected polarisation dichotomy is still not reproduced.

Therefore, the two phase model needs to be further refined.

So, as expected from observations, brightest fluxes are produced for unobscured, type-1 viewing angles but the model fails to reproduce neither acceptable levels of polarisation nor the observed polarisation dichotomy. Some morphological modifications must be considered to aim for polarisation degrees of the order of 1 % and 5 % at type-1 (Smith et al. 2002) and type-2 (Kay 1994) inclinations, respectively.

2.4.2 Investigating different opening angles

Similarly to Sect. 2.3, we now explore a broader range of morphological parameters (θ , $\delta\theta$) in order to discriminate between more realistic and less favourable realisations of the two-phase wind model. As seen from Fig. 8, the polarisation continuum is close to being wavelength-independent, thus we will also plot the wavelength-integrated polarisation degree as a function of the viewing angle. The sign convention is preserved from Sect. 2.3.

For $\theta = 60^\circ$ (Fig. 9), the model uniformly creates negative (parallel) polarisation for the whole range of half-opening angles, with moderate polarisation degrees at low inclinations, increasing up to 12 % at equatorial viewing angles. The parametrisation is non compatible with the expected polarisation dichotomy. However, the case of $\theta = 45^\circ$ is more interesting as it correctly reproduces the variation of the polarisation position angle between type-1 and type-2 inclinations. The transition between negative to positive polarisation is a function of the half-opening angle of the model, but is comprised between $i \sim 34^\circ$ and $i \sim 42^\circ$. Negative [positive] polarisation degrees reach up to 1.2 % [25.6 %] for the flattest flow geometry ($\delta\theta = 3^\circ$) and the polarised flux tends to decrease when the observer's line-of-sight is reaching the equatorial plane ($P = 16.3$ %). Finally, for $\theta = 30^\circ$, the polarisation dichotomy also appears but the regime transition occurs between $i \sim 15^\circ$ and $i \sim 24^\circ$, which is unrealistic according to the observed distribution of AGN types and individual observations of Seyfert-1 inclinations, such as for ESO 323-G077 ($i = 45.0^\circ$, Schmid et al. 2003) or NGC 5548 ($i = 47.3_{-6.9}^{+7.6}$, Wu & Han 2001). Moreover, the polarisation degree for models with $\theta = 30^\circ$ can be as high as 62 % at equatorial inclinations, a behaviour far from polarimetric observations of obscured AGN (Kay 1994).

Our immediate conclusions are coherent with the ones derived from electron-filled outflowing models presented in Sect. 2.3 : a model with a wind bending angle $\theta = 60^\circ$ unsuccessfully reproduces the polarisation dichotomy, but a change in the flow geometry can solve this issue. As stated in Sect. 2.3, immediate observational tests for the number of BAL, NAL, and non-NAL quasars can be performed to test the possible angles θ and $\delta\theta$. In particular, for $\theta = 45^\circ$, both the transition between parallel and perpendicular polarisation at acceptable inclinations and polarisation degree close to observed quantities are emerging (non-NAL quasars polarisation ~ 1 %, NAL-objects ~ 16 % and BALQSO's ~ 25 %). The transition regime between type-1 and type-2 signatures appears to be below $i = 45^\circ$, which is in agreement

with the inclination of borderline type-1 objects (Schmid et al. 2003).

2.4.3 Exploring a range of dust optical depths

It remains a challenge to the double-wind model to reproduce the observed levels of polarisation. With respect to the results of Sect. 2.4.2, the polarisation degree should be reduced by a factor of five at type-2 inclinations, and by a factor of two at intermediate viewing angles. The cold, absorbing medium shielded by the WHIM may play a decisive role in this.

In our first test, we fixed the absorbing equatorial optical depth to 40, which may be an upper limit for the medium opacity. A wider range of τ_{dust} is now investigated in Fig. 10, varying proportionally τ_{dust} from 40 to 0.4 (40, 4, 1, 0.4). The figure shows a series of intermediate cases between our results for an optically thick dust layer explored in the previous Sect. 2.4.2 and the pure WHIM case (Sect. 2.2).

As seen from Fig. 9, at high optical depths of the dust, the scenarios of Fig. 10 have similar polarimetric properties to the multi-component torus models investigated in Marin et al. (2012). The polarisation dichotomy is reproduced but the polarisation degree at type-2 inclinations is higher than observed P levels (Kay 1994). Decreasing the dust optical depth ($\tau_{dust} = 4$) diminishes the overall P as photons can now escape from the dusty funnel by transmission through the dust wind. The polarisation dichotomy is preserved down to τ_{dust} approximately equals unity, where the multiple regimes for parallel and perpendicular polarisation reappear. However, they leave a higher covering factor for the observed number density of type-2 AGN and the resulting polarisation degree at equatorial viewing angles is lower and thus closer to the observed range. Our modelling excludes optically thin dust environments ($\tau_{dust} < 1$) as they automatically generate parallel photon polarisation angles at equatorial inclinations.

The impact of the model morphology is essentially visible at intermediate and equatorial viewing angles, where the observer's line-of-sight is crossing the dust material. For type-1 objects, the polarisation degree is found to be parallel, with $P < 2$ %, slightly increasing with i . Around 45° , P remains stable for a few i , depending on the half-opening angle of the outflow. Such a polarisation plateau ($P \sim 3 - 5$ %) associated with a perpendicular polarisation position angle is a strong observational prediction that could help to estimate the average $\delta\theta$ of BAL-quasars². For higher inclinations, P rises as backscattered photons from the WHIM funnel strongly contributes to the polarisation flux. When the internal structure becomes hidden by the cold, outer dust layer, P starts to decrease until it reaches a minimal value along type-2 inclinations (below 10 % at $\tau_{dust} \leq 4$).

We thus find that for $\theta = 45^\circ$, and $\delta\theta = 3^\circ - 10^\circ$, and

² Our predictions seem to be supported by the spectropolarimetric observations performed on 6 individual BAL QSO by Lamy & Hutsemekers (2004a,b), where P is found to be of the order of a few percents, associated with a perpendicular polarisation position angle for 4 out of 6 objects.

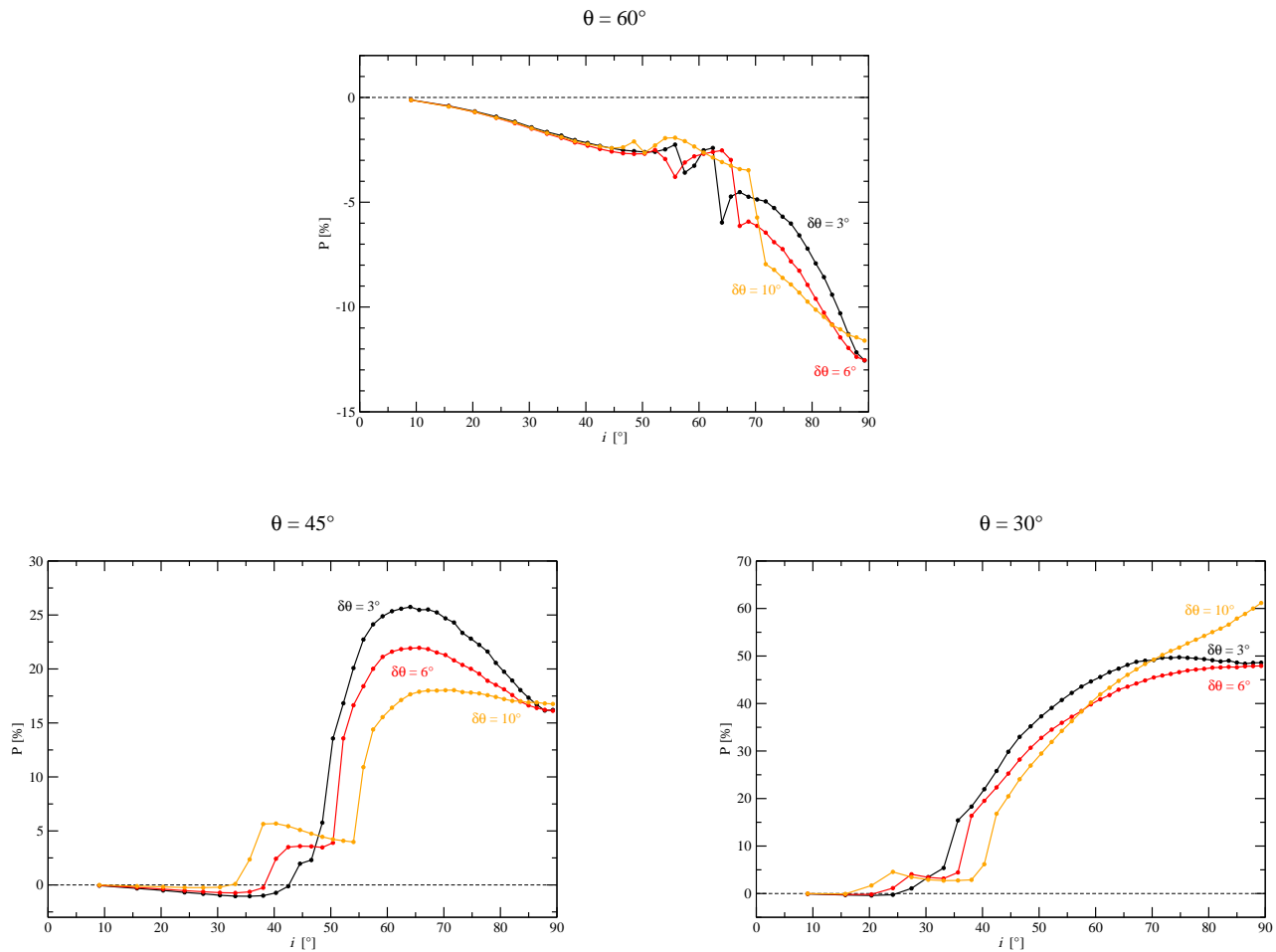


Figure 9. Investigating the polarisation response of the dual quasar’s structure according to the observer’s viewing angle i , at three different wind bending angles θ and three outflow’s opening angle $\delta\theta$ (black : $\delta\theta = 3^\circ$ – red : $\delta\theta = 6^\circ$ – orange : $\delta\theta = 10^\circ$). *Top*: $\theta = 60^\circ$; *bottom-left*: $\theta = 45^\circ$; *bottom-right*: $\theta = 30^\circ$.

moderate optical depths of the dust with $1 < \tau_{dust} \leq 4$, the double-wind model seems to rather well reproduce the observed continuum polarisation. It gives strong observational predictions on the geometrical opening angles of the outflow, as well as the amount of cold dust that can survive so close from the emitting source. However, it is important to investigate if the physical and geometrical changes to the model of Elvis (2000) proposed are realistic and in agreement with number counts of different AGN types.

3 DISCUSSION

3.1 Summarising our study of the outflow model

We tested to which extent the WHIM model of Elvis (2000) can reproduce the observed polarisation dichotomy with respect to the polarisation position angle, as well as the expected level of polarisation percentage in type-1 and type-2 AGN. A pure Thomson scattering model with $\theta = 60^\circ$ and $\delta\theta = 3^\circ$ presents low P levels ($< 1\%$) and cannot reproduce the perpendicular polarisation expected at equatorial incli-

nations. For low-luminosity objects, Elvis (2000) predicts that the amount of polarisation along the outflow’s direction, where a layer of dust prevents the detection of BAL, would be below 0.5 %. Our modelling agrees with this claim but adding dust to the outer parts of the conical outflows still does not produce the expected polarisation dichotomy. Finally, a double-layered wind also solely produces parallel polarisation, as well as too high polarisation percentages at type-2 viewing angles.

Exploring different sets of morphological and opacity parameters, we then found that small modifications help to match the modelling results with polarisation observations. A key point is to slightly lower the bending angle of the winds ($\theta_{60^\circ} \rightarrow \theta_{45^\circ}$) to allow for the presence of perpendicular polarisation at type-2 viewing directions. Perpendicular polarisation at intermediate and equatorial lines-of-sight emerges naturally when photons travel through geometrically thick regions with an optical depth equal or larger than unity.

For the pure WHIM model we found parametrisations that may correspond to the observed polarisation di-

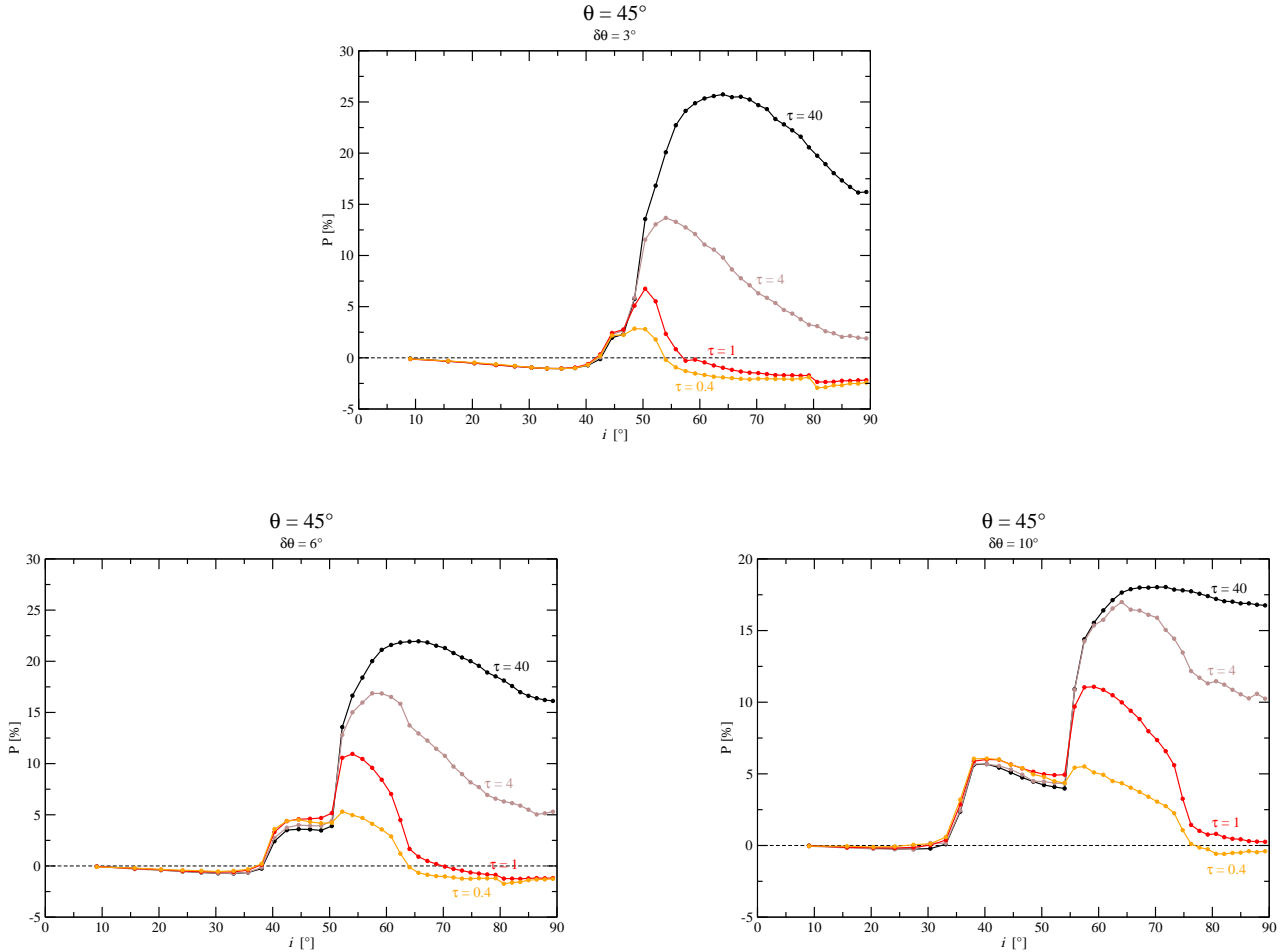


Figure 10. Investigating the polarisation response of the dual quasar’s structure with a bending angle $\theta = 45^\circ$ according to the observer’s viewing angle i , varying the outflow’s opening angle $\delta\theta$ and the dust equatorial optical depth τ (black : $\tau_{dust} = 40$ – brown : $\tau_{dust} = 4$ – red : $\tau_{dust} = 1$ – orange : $\tau_{dust} = 0.4$). *Top*: $\delta\theta = 3^\circ$; *bottom-left*: $\delta\theta = 6^\circ$; *bottom-right*: $\delta\theta = 10^\circ$.

chotomy between non-NAL/NAL (type-1) AGN and obscured BALQSO’s or Seyfert-2 galaxies. However, the solid angle of the sky covered by Seyfert-2 galaxies may require additional dust obscuration that we also tested. Both, the observed polarisation dichotomy and polarisation degrees can be reproduced if we consider a dual wind model with $\theta = 45^\circ$ and include equatorial scattering in the accretion flow. The half-opening angle $\delta\theta$ of the flow then normalises the polarisation degree as well as the maximum inclination at which parallel polarisation is still detected. The opacity of the outer (dusty) wind may also be adjusted to decrease the polarisation degree at equatorial inclinations; the maximum polarised flux is then observed along the outflowing direction. To match with spectropolarimetric observations, the dust optical depth along the equator should be close to unity.

3.2 Discriminating between different wind models

The question of discriminating between different wind models was raised by Elvis (2000, 2002a,b) discussing wind prop-

erties for the X-ray range. We here add a brief discussion about the UV/optical properties of the ionisation cones and narrow line regions seen in Seyfert-2 like galaxies. The first conical models were based upon the geometrical shape of the extended narrow line regions that are supposed to be the natural extension of the ionised outflows. The assumed morphology is an hourglass-shaped, bi-conical region with the emitting source situated at the cone base.

The resulting polarisation rises from face-on towards edge-on viewing angles and uniquely produces perpendicular polarisation angles, independently of the filling medium (either electrons or dust grains, Goosmann & Gaskell 2007). Typically, P can be as high as 20 % for ionised or dusty winds. However, the wind structure of Elvis (2000) presents a very different polarisation pattern: in contrast to polar outflows, the hollow winds can produce polarisation at parallel and perpendicular position angles. Compared with the model presented in Fig. 9 and Fig. 10, the polarisation degree is small ($P < 5\%$) at both polar and equatorial viewing angles. The maximum polarisation degree is reached for lines-of-sight crossing the outflow, with $5 < P < 25\%$, de-

pending on the model's dust opacity and half-opening angle. The two-phase model succeeds to reproduce the polarisation degree expected from the polarised continuum of BAL quasars (Cohen et al. 1995; Goodrich & Miller 1995; Ogle 1998).

The low-luminosity version of the wind with dusty extensions leads to $P < 0.5\%$ as predicted for non-BAL objects (Berriman et al. 1990). Moreover, Elvis (2000)'s two-phase model may produce a polarisation position angle that varies from 90° at pole-on views to 0° at equatorial views, which is in agreement with the observed polarisation dichotomy. Depending on the parametrisation, it is also possible to create $\psi = 0^\circ$ photons at polar inclinations – a phenomenon observed in some Seyfert-1 galaxies that were named *polar scattering dominated* AGN by Smith et al. (2002).

3.3 Polarisation upper limits from Seyfert-atlases

Compared to the modelling results for AGN winds, the observed polarisation degrees are generally found to be significantly lower. In the atlas of Seyfert-2 galaxies presented by Kay (1994), a large polarisation degree was detected for Mrk 463E ($P = 10.29 \pm 0.18\%$ after starlight correction, $z = 0.050$ Veron-Cetty & Veron 1987), but finding such highly polarised type-2 AGN is quite uncommon. The majority of the observed Seyfert-2 galaxies show lower P values, usually below 3% (Miller & Goodrich 1990; Kay 1994). Most Seyfert-1 galaxies have much weaker polarisation degrees, usually below 1% (Smith et al. 2002, 2004), except for exceptional, high-polarisation objects where P can reach up to 5% (see Mrk 231 in Goodrich & Miller 1994 and Fairall 51 in Smith et al. 2002).

The diversity of detected polarisation degrees is difficult to assess in the modelling. Simulations of simple and isolated (Miller & Goodrich 1990), or complex and radiatively coupled (Marin et al. 2012; Marin & Goosmann 2012) reprocessing regions in AGN tend to create too large polarisation degrees at equatorial viewing angles and not enough polarisation at polar inclinations. The outflow model evaluated in this paper seems to be able to overcome these difficulties when taking into account a two-phase wind structure. High polarisation degrees at a perpendicular polarisation position angle can be reached if the inclination of the system is close to the bending angle of the quasar wind; low P values are produced when the observer's line-of-sight is close to the equatorial plane. As the proposed set of outflow half-opening angles lies between 3° and 10° , the ratio of high- P to low- P AGN remains small, which is coherent with the few high- P Seyfert-2 galaxies detected so far. As for Seyfert-1 galaxies, the structure is able to produce parallel polarisation as high as 2% (Fig. 9), while preserving the observational evidence of higher P values for equatorial viewing angles than at polar inclinations (Fig. 9 and Fig. 10).

3.4 The test case of the Seyfert galaxy NGC 5548

NGC 5548 is one of the best laboratories for testing AGN models (Rokaki et al. 1993) and an important reference for Elvis (2000). How does the wind model hold against spectropolarimetric measurements of the object? The Seyfert-1 galaxy ($z = 0.0174$) shows a continuum polarisation degree

of $0.67 \pm 0.01\%$ associated to a position angle of $\psi \sim 45.6 \pm 0.6^\circ$ (Goodrich & Miller 1994)³. To compare our modelling predictions to the measured polarisation position angle, the observed ψ needs to be related to the position angle of the radio axis of NGC 5548 (157°). The angular difference of 111° is roughly perpendicular.

According to Goodrich & Miller (1994), perpendicular polarisation indicates that polar electron scattering is the dominant scattering mechanism. However, Wu & Han (2001)'s estimation of the inclination towards NGC 5548 ($i = 47.3^\circ \pm_{-6.9}^{+7.6}$) implies that the polarisation degree should be significantly higher than the observed value. Our model presented in Fig. 7 can explain the polarisation degree and the polarisation position angle of NGC 5548 in the context of the wind model for a bending angle of 45° . It strengthens the idea that AGN winds do not need to be fully filled by reprocessing matter; a hollow geometry may be then considered as more likely.

3.5 The morphology of the outflow in IC 5063

Located in the southern hemisphere, IC 5063 ($z = 0.011$, Morganti et al. 2007) is a Seyfert-galaxy that is famous to be the first AGN where a fast outflow of neutral hydrogen was detected (Morganti et al. 1998). Among other characteristics, its *Hubble Space Telescope* image shows an ionised structure extending out to 15 kpc in a remarkable, X-shaped morphology (Morganti et al. 2003). However, spectroscopic and spectropolarimetric images of solid double cone models (Wolf & Henning 1999; Marin et al. 2012) show that the scattering region re-emits uniformly to the irradiation source and the peculiar behaviour of IC 5063 cannot be visually explained using uniform or fragmented polar winds. The idea that AGN winds may be hollow came while observing the 3-dimensional velocity field of the line-emitting gas over 1 kpc in NGC 1365 (Hjelm & Lindblad 1996). The flow pattern of such a wind then naturally creates an X-shaped signal in the imaging.

The WHIM model investigated in this paper (Fig. 3 bottom) successfully reproduces⁴ the X-shaped morphology of IC 5063, as well as the bright flux spot in the AGN inner regions detected by Morganti et al. (2003). It indicates that Thomson scattering is still a dominant mechanism at large distances from the central source of IC 5063 and it tends to support the idea that quasar outflows are hollow structures. However, not all AGN where hollow winds are suggested show an X-shaped morphology (see for instance NGC 2992 in Veilleux et al. (2001) or NGC 1068 in Crenshaw & Kraemer (2000)). A possible complication here may be that the amount of dust in the extended narrow line regions is high and thus prevents direct imaging of the hollow wind signatures.

³ In comparison, Smith et al. (2002) found $P \sim 0.69 \pm 0.01\%$ and $\psi \sim 33.2 \pm 0.5^\circ$ for NGC 5548

⁴ The *Hubble Space Telescope* image presented by Morganti et al. (2003) is based on total flux only, while our Fig. 3 shows the polarised flux (total flux \times polarisation degree). We checked that the X-shape morphology is also reproduced in total flux, a straightforward conclusion as Thomson scattering is wavelength-independent.

3.6 The tilted outflow of NGC 1068

NGC 1068 is considered to be one of the most archetypical examples of thermal Seyfert-2 galaxies. According to the simplest approach in AGN unification models (Antonucci 1993; Urry & Padovani 1995), the central region of NGC 1068 is hidden by optically thick, circumnuclear matter usually designated as a dusty torus. It is then a direct consequence of the circumnuclear dust that the radiation of the central engine escapes non-isotropically along the polar regions. It forms the so-called ionised winds that farther out interact with the interstellar medium of the host galaxy and give rise to narrow emission lines (Osterbrock & Mathews 1986). It is a common hypothesis that as a consequence of the collimation effect by the circumnuclear dust the polar outflows sustain the same half-opening angle as the dusty torus. This assumption is derived from the assumed axisymmetry of the unified model. However a recent study on NGC 1068 carried out by Raban et al. (2009) showed that the polar winds (represented by a bi-conical structure) are most likely inclined with respect to the obscuring torus axis. In the context of this work, several models of tilted outflows (Das et al. 2006; Goosmann & Matt 2011; Marin et al. 2012) are being developed – but the off-axis outflow may also be explained by the structure for quasars if the radiation pressure field is not isotropic. In this case, the bending of the flow becomes non-axisymmetric and the extended outflow would appear tilted with respect to the symmetry axis of the system.

4 CONCLUSIONS AND FUTURE WORK

Conducting detailed radiative transfer simulations that include polarisation, we show that the structure for quasars suggested by Elvis (2000) can reproduce the observed optical polarisation properties of type-1 and type-2 AGN if the standard version of the model is slightly modified: the bending angle of the wind should be lowered to $\theta = 45^\circ$ and a dusty phase of moderate optical depth should be added to the wind.

Without the dusty phase, i.e. for a pure WHIM outflow, the polarisation dichotomy of Seyfert galaxies may still be reproduced for a certain, rather specific range of parameters but the predicted number density of type-2 AGN would turn out too low.

The modelling leads to some straightforward observational tests and future work:

(i) The bending angle and covering factor of the extended winds that we derive from the polarisation modelling imply number densities for non-NAL and NAL AGN, BALQSO's, as well as type-1 versus type-2 AGN. Such number counts can be derived from multi-waveband data obtained in large sky surveys (e.g. Roseboom et al. 2013), as the distribution of covering factors is correlated with the fraction of IR luminosity. It is thus possible to test if the observed distribution of different AGN types corresponds to their polarisation properties, and a preliminary investigation of the inclination-dependency of AGN spectropolarimetric observations is ongoing.

(ii) So far, our modelling only refers to UV/optical continuum radiation. Computations for emission and absorption lines that also consider different velocity fields inside the wind are currently under way. Furthermore, we intend to extend the modelling towards the X-ray regime and to compare the results to X-ray spectroscopy data.

(iii) The exact wind geometry varies most likely with the bolometric luminosity of the AGN. Therefore, it is useful to study the polarisation properties of well-observed, individual AGN with different average luminosities and to derive the resulting angles θ and $\delta\theta$ for the two-phase wind model. Possible trends of θ and $\delta\theta$ with the luminosity can thus be investigated.

It is interesting to note that, from a purely morphological point of view, the two-phase version of the wind model by Elvis (2000) is not in disagreement with the standard scenario of the unified scheme as analyzed in Marin et al. (2012). Nonetheless, it is a major difference between the two interpretations to assume that the obscuring material originates in a wind instead of being part of the accretion inflow.

ACKNOWLEDGMENTS

The authors are grateful to the referee Makoto Kishimoto for his useful and constructive comments on the manuscript. This research was funded by the French grant ANR-11-JS56-013-01 of the project POLIOPTIX. The authors are grateful to Delphine Porquet for clarifying comments on the manuscript.

REFERENCES

- Antonucci, R. R. J. 1983, *Nature*, 303, 158
- Antonucci, R. R. J. 1984, *ApJ*, 278, 499
- Antonucci, R. R. J., & Miller, J. S. 1985, *ApJ*, 297, 621
- Antonucci, R. 1993, *ARA&A*, 31, 473
- Axon, D. J., Capetti, A., Macchetto, F., Sparks, W. B., & Boksenberg, A. 1996, *Vistas in Astronomy*, 40, 29
- Bentz, M. C., Walsh, J. L., Barth, A. J., et al. 2009, *ApJ*, 705, 199
- Berriman, G., Schmidt, G. D., West, S. C., & Stockman, H. S. 1990, *ApJs*, 74, 869
- Capetti, A., Axon, D. J., Macchetto, F., Sparks, W. B., & Boksenberg, A. 1995, *ApJ*, 446, 155
- Cohen, M. H., Ogle, P. M., Tran, H. D., et al. 1995, *ApJl*, 448, L77
- Crenshaw, D. M., & Kraemer, S. B. 2000, *ApJl*, 532, L101
- Czerny, B., & Hryniewicz, K. 2012, *Journal of Physics Conference Series*, 372, 012013
- Das, V., Crenshaw, D. M., Kraemer, S. B., & Deo, R. P. 2006, *AJ*, 132, 620
- Davidson, K., & Netzer, H. 1979, *Reviews of Modern Physics*, 51, 715
- Edelson, R. A., Malkan, M. A., & Rieke, G. H. 1987, *ApJ*, 321, 233
- Elvis, M., 2000, *ApJ*, 545, 63
- Elvis, M. 2002, *Mass Outflow in Active Galactic Nuclei: New Perspectives*, 255, 303
- Elvis, M. 2002, *Issues in Unification of Active Galactic Nuclei*, 258, 51

- Elvis, M. 2012, *AGN Winds in Charleston*, 460, 186
- Eracleous, M. 2006, *Astronomical Society of the Pacific Conference Series*, 360, 217
- Fath, E. A. 1909, *Lick Observatory Bulletin*, 5, 71
- Gaskell, C. M. 2009, *NewAR*, 53, 140
- Gaskell, C. M., & Goosmann, R. W. 2013, *ApJ*, 769, 30
- Goodrich, R. W., & Miller, J. S. 1994, *ApJ*, 434, 82
- Goodrich, R. W., & Miller, J. S. 1995, *ApJl*, 448, L73
- Goosmann, R. W., & Gaskell, C. M. 2007, *A&A*, 465, 129
- Goosmann, R. W., & Matt, G. 2011, *MNRAS*, 415, 3119
- Hjelm, M., & Lindblad, P. O. 1996, *A&A*, 305, 727
- Kay, L. E. 1994, *ApJ*, 430, 196
- Kishimoto, M. 1999, *ApJ*, 518, 676
- Kishimoto, M., Kay, L. E., Antonucci, R., et al. 2002, *ApJ*, 567, 790
- Kishimoto, M., Antonucci, R., & Blaes, O. 2003, *MNRAS*, 345, 253
- Kishimoto, M., Antonucci, R., Boisson, C., & Blaes, O. 2004, *MNRAS*, 354, 1065
- Kishimoto, M., Hönig, S. F., Beckert, T., & Weigelt, G. 2007, *A&A*, 476, 713
- Kishimoto, M., Antonucci, R., Blaes, O., et al. 2008, *Nature*, 454, 492
- Lamy, H., & Hutsemékers, D. 2004, *A&A*, 427, 107
- Lamy, H., & Hutsemékers, D. 2004, *VizieR Online Data Catalog*, 342, 70107
- Marin, F., Goosmann, R. W., Gaskell, C. M., Porquet, D., & Dovčiak, M. 2012, *A&A*, 548, A121
- Marin, F., & Goosmann, R. W. 2012, *SF2A-2012: Proceedings of the Annual meeting of the French Society of Astronomy and Astrophysics*, 587
- Marin, F., Goosmann, R., & Dovčiak, M. 2012, *Journal of Physics Conference Series*, 372, 012065
- Mathews, W. G., & Capriotti, E. R. 1985, *Astrophysics of Active Galaxies and Quasi-Stellar Objects*, 185
- Mathis, J. S., Rumpl, W., & Nordsieck, K. H. 1977, *ApJ*, 217, 425
- Miller, J. S., Goodrich, R. W., & Mathews, W. G. 1991, *ApJ*, 378, 47
- Morganti, R., Oosterloo, T., Holt, J., Tadhunter, C., & van der Hulst, J. M. 2003, *The Messenger*, 113, 67
- Morganti, R., Oosterloo, T., & Tsvetanov, Z. 1998, *AJ*, 115, 915
- Morganti, R., Holt, J., Saripalli, L., Oosterloo, T. A., & Tadhunter, C. N. 2007, *A&A*, 476, 735
- Miller, J. S., & Goodrich, R. W. 1990, *ApJ*, 355, 456
- Ogle, P. M. 1998, Ph.D. Thesis,
- Ogle, P. M., Brookings, T., Canizares, C. R., Lee, J. C., & Marshall, H. L. 2003, *A&A*, 402, 849
- Ogle, P. M., Cohen, M. H., Miller, J. S., et al. 1999, *ApJS*, 125, 1
- Osterbrock, D. E., & Mathews, W. G. 1986, *ARA&A*, 24, 171
- Osterbrock, D. E. 1991, *Reports on Progress in Physics*, 54, 579
- Packham, C., Young, S., Hough, J. H., Axon, D. J., & Bailey, J. A. 1997, *MNRAS*, 288, 375
- Raban, D., Jaffe, W., Röttgering, H., Meisenheimer, K., & Tristram, K. R. W. 2009, *MNRAS*, 394, 1325
- Roseboom, I. G., Lawrence, A., Elvis, M., et al. 2013, *MNRAS*, 429, 1494
- Rokaki, E., Collin-Souffrin, S., & Magnan, C. 1993, *A&A*, 272, 8
- Schmid, H. M., Appenzeller, I., & Burch, U. 2003, *A&A*, 404, 505
- Shakura, N. I., & Sunyaev, R. A. 1973, *A&A*, 24, 337
- Shields, G. A. 1977, *ApL*, 18, 119
- Smith, J. E., Young, S., Robinson, A., et al. 2002, *MNRAS*, 335, 773
- Smith, J. E., Robinson, A., Alexander, D. M., et al. 2004, *MNRAS*, 350, 140
- Suganuma, M., Yoshii, Y., Kobayashi, Y., et al. 2006, *ApJ*, 639, 46
- Urry, C. M., & Padovani, P. 1995, *PASP*, 107, 803
- Veilleux, S., Shopbell, P. L., & Miller, S. T. 2001, *AJ*, 121, 198
- Veron-Cetty, M.-P., & Veron, P. 1987, *ESO Scientific Report, Garching: European Southern Observatory (ESO)*, 1987, 3rd ed.,
- Wolf, S., & Henning, T. 1999, *A&A*, 341, 675
- Wu, X.-B., & Han, J. L. 2001, *ApJL*, 561, L59
- Young, S., Hough, J. H., Axon, D. J., Bailey, J. A., & Ward, M. J. 1995, *MNRAS*, 272, 513